Dimension Reduction Approach for Understanding Resource-Flow Resilience to Climate Change

Ariel Salgado[1,*], Yiyi He[2], John Radke[1,2], Auroop Ganguly[3,4], and Marta C. Gonzalez[1,5,+]

[1]Department of City and Regional Planning, University of California at Berkeley, Berkeley, CA 94720, USA
[2]Department of Landscape Architecture and Environmental Planning, University of California at Berkeley, Berkeley, CA 94720, USA
[3]Pacific Northwest National Laboratory, Richland, WA, USA
[4]Sustainability and Data Sciences Laboratory, Department of Civil and Environmental Engineering, Northeastern University, Boston, MA, USA
[5]Department of Civil and Environmental Engineering, University of California at Berkeley, Berkeley, CA 94720, USA
[*]arielolafsalgado@gmail.com
[+]martag@berkeley.edu

ABSTRACT

Networked dynamics are essential for assessing the resilience of lifeline infrastructures. The dimension-reduction approach was designed as an efficient way to map the high-dimensional dynamics to a low-dimensional representation capturing system-level behavior while taking into consideration network structure. However, its application to socio-technical systems has not been considered yet. Here, we extend the dimension-reduction approach to resource-flow dynamics in multiplex networks. We apply it to the San Francisco fuel transportation network, considering the flow between refineries, terminals and gas stations. We capture the aggregated dynamics between the facilities of each type and identify macroscopic conditions for the system to supply a given demand of fuel. By considering multiple sea level rise scenarios between 2020 and 2100, we address the impact of coastal flooding due to climate change on the maximum suppliable demand. Finally, we analyze the system's transient response to production failures, investigating the temporary interruption in production and the duration it takes for complete demand satisfaction to become unachievable after the interruption.

Introduction

In recent years, the topic of system resilience has gained more attention from the scientific community[1–4], as the effects of climate change become more evident in the world around us[5–7]. Climate change exposes lifeline systems to unexpected levels and types of stress, endangering their functionality. Resilience analysis considers the dynamical behavior of a system during a failure, by considering its different stages: preparation, robustness and recovery[2]. One possible approach to assess resilience is based on Dynamical Systems theory, usually through changes in the parameters describing the system at different scenarios. However, traditional Dynamical Systems methodologies may require a detailed description of system dynamics, unfeasible in many cases. Techniques have been developed to partially overcome this limitation, by working with general, broadly defined functions, seeking to understand a system's behavior around its stable state[8,9]. As the system scale increases and interaction patterns become more complex, network-based approaches have become crucial to model a system's topology, and assess the impact of changes on its structure[1,2,10]. By combining network structure and dynamics, the dimension-reduction approach[11–14] provides a tool to assess system dynamics at large scale, while taking into account the patterns of interactions between the system's constituents. Originally developed in the context of ecology, the approach focuses on generating a low-dimension set of equations capturing the macroscopic behavior of the system, through only a few equations (compared to the original system size). The parameters appearing in the reduced set of equations capture the network topology, and help analyze the impact of network structure on system dynamics.

In this work, we extend the dimension-reduction approach[11–14] to the context of resource-flow networks. Resource-flow networks[15] comprise those networked systems where some quantity is transported from one part of a system to another, following conservation laws. Resource-flow dynamics include many examples from urban systems, as supply chain management[9,16], disease propagation[17], water distribution[18], and trade relationships[19]. Here, we consider a case study from supply chains: the San Francisco Fuel Transportation Network (SFFTN). We examine the influence of climate change on the SFFTN, and we delve into the ramifications of Sea Level Rise (SLR)[20] as detailed in He et al.[21].

Supply chain dynamics can be challenging, as they are heavily dependent on various levels of human decision and

environmental factors. Future demand estimation has been considered, through the use of difference equations[16,22] finding how demand variation increases from consumers to producers (known as the bullwhip effect). Ordinary differential equations have been used to model supply chain dynamics from a coarsen perspective[9], since they treat flow as a continuous magnitude, and thus they are not suited to capture events in very small scales of time. Information privacy on flows between firms limits modeling, as only little data is available for comparison. Here, we study resource-flow networks under simple dynamics capturing the qualitative behavior of supply and demand, and the general conditions for stability induced by network topology. Instead of looking for a detailed description of each facility within the network, we focus on a system-level scale, through the dimension-reduction approach. By considering refineries, terminals, and gas stations included within the SFFTN, we write down a set of ordinary differential equations representing the flow of fuel from refineries to gas stations. Then, we obtain a dimensionally reduced description of the system by considering the average amount of fuel stored at each type of facility.

We use the approximation to analyze the impact of coastal flooding on the transportation system, by considering its ability to supply demand under different climate change scenarios. Later, we consider the ability of the system to sustain demand during a production failure, under different coastal flooding scenarios between years 2020 and 2100. The results depict the transition of the system through different stages of failure, up to the point of it being unable to satisfy any level of demand. By considering both the impact of topology alone and through simple dynamical laws capturing transportation's qualitative behavior, our approximation provides an estimate of the maximum demand that could be sustained under multiple SLR scenarios. Our work constitutes three different contributions to the topic of resilience of networked dynamical systems. First, the dimension-reduction approach shows the conditions imposed over the space of stable flows by the network structure. Second, by studying lifeline infrastructure systems such as the SFFTN, we extend the dimension-reduction approach to the context of socio-technical systems. Lastly, by considering the impact of SLR through climate change scenario analysis, we study a realistic example of failure from a dynamical systems perspective.

Results

The San Francisco Fuel Transportation Network and the effects of coastal flooding

The SFFTN was presented originally in He et al.[21]. It was constructed by considering spatial information from OpenStreetMaps and Google Places, the California Energy Commission (CEC), and the companies involved in fuel production and transportation in the region. It includes two types of nodes, corresponding to transportation means (railway, sea, road, oil and product pipelines), and facilities (ports, terminals, refineries, gas stations and airports). We simplify this complex structure by representing it as a multiplex network where nodes are facilities (and each layer corresponds to a type of facility) and transportation means correspond to different types of links between the layers. For the purpose of this work, we focus on the subnetwork supporting the transportation from refineries (production points) to terminals (intermediate storage points) and gas stations (consumption points). Refineries and terminals connect through product pipelines, in a structure that allows flow between any pair of them. Both of them connect to gas stations through the road network, which allows transportation from any refinery or terminal to any gas station. The majority of the flow goes from refineries to terminals through product pipelines, and from terminals to gas stations through trucks. A smaller portion of the fuel is directly transported from refineries to gas stations through trucks. The spatial representation of the SFFTN can be found in Fig. 1 a, and its network abstraction in Fig. 1 d.

Due to the effect of climate change, coastal regions in the San Francisco Bay Area (SFBA) are likely to flood frequently in the next hundred years[23]. Through the use of computational modeling, scenario analysis has been used to assess the impact of coastal flooding on the systems located within the region[23]. Using the flooding scenarios constructed in Radke et al.[23], we consider four different time horizons (2020-2040, 2040-2060, 2060-2080, and 2080-2100), under two Representative Concentration Pathways (RCPs, 4.5 and 8.5)[24]. For each, four global climate or earth system models (GCM) are used to produce predictions of typical, high, and extreme SLR at the SFBA, corresponding to the 50, 95, and 99.9 percentiles of the SLR predicted by each model and for each location at the SFBA. The models are CanESM2, MIROC5, CNRM-CM5 and HadGEM2-ES, corresponding to the CMIP5 suite of models[25]. Water column height estimations are constructed through the 3Di hydrodynamic model[26]. Further details are provided in the Methods section. Fig. 1 a-f depicts the impact of SLR on time horizons 2060-2080 and 2080-2100 for RCP 8.5 and the 99.9 SLR percentile, where it is more appreciable. A region is considered flooded under a given scenario if the water column at that region is higher than $15cm$. Coastal flooding can be appreciated in the spatial representation (Figs. 1 a-c). Nodes at flooded locations are removed from the network, as they are considered failed. In the abstract representation (Figs. 1 d-f), it is evident how coastal flooding largely reduces the number of terminals and product pipelines, while also reducing the number of refineries in the last time horizon. The effect of coastal flooding is not only to remove facilities, but also to disconnect them from the different layers. This impacts the flow capacities between the layers, reducing the ability of the refineries to transmit the produced fuel to the terminals and gas stations. See Methods section for more detail on the change of the network structure due to coastal flooding.

Dynamical representation

We start by considering a set of ordinary differential equations describing fuel transportation, produced at refineries, transported to terminals, and then to gas stations (the main path of flow) or directly to gas stations (a secondary path of flow). Usually, production, consumption, and flow between facilities will depend on the stock level they have at a given moment. To describe the state of the system, we consider variables $x_i^q \in [0,1]$, indicating the stock level at facility $i = 1,\ldots.N_q$ in layer $q = 1,2,3$ (corresponding to refineries, terminals, and gas stations, respectively). We consider that nodes in layer q have stock capacity C^q, and so the resource stored at it is $C^q x_i^q$. We assume that production at a refinery and consumption at a gas station only depend on their individual stock levels, and that flow between facilities only depends on the stock levels of the facilities involved. Then the dynamics of the stock levels are described by

$$\begin{aligned}
C^1 \dot{x}_i^1 &= P\Pi(x_i^1) - \sum_{j=1}^{N_2} W_{ij}^{12}\Psi(x_i^1, x_j^2) - \sum_{j=1}^{N_3} W_{ij}^{13}\Psi(x_i^1, x_j^3) \\
C^2 \dot{x}_i^2 &= \sum_{j=1}^{N_1} W_{ji}^{12}\Psi(x_j^1, x_i^2) - \sum_{j=1}^{N_3} W_{ij}^{23}\Psi(x_i^2, x_j^3) \\
C^3 \dot{x}_i^3 &= -D\Delta(x_i^3) + \sum_{j=1}^{N_1} W_{ji}^{13}\Psi(x_j^1, x_i^3) + \sum_{j=1}^{N_2} W_{ji}^{23}\Psi(x_j^2, x_i^3)
\end{aligned} \tag{1}$$

where:

- $\Pi(x_i^1) \in [0,1]$ is the production level at refinery i, and P is the production capacity (maximum production possible) of a refinery.
- $\Delta(x_i^3) \in [0,1]$ is the demand level at gas station i, and D is the maximum demand that can be supplied by a gas station.
- $\Psi(x_i^q, x_j^r)$ is the flow level from facility i in layer q to facility j in layer r, and W_{ij}^{qr} is the flow capacity between them.

Notice the similarity of Eq. 1 with the Barzel-Barabasi equation[27], considered in the original application of the dimension-reduction approach[11]. However, in the context of resource-flow systems, the interaction term appears with a different sign at the different ends of the flow, and thus the interaction term is different at each layer. One of the main difficulties when working with supply chains connecting multiple firms is that detailed information on their transportation policies and capacities is often unavailable. In the case of the SFFTN, reasonable values for the system's parameters can be found in an aggregated fashion through the CEC, as described in the Methods section. To address the uncertainty in the parameter values, we consider ranges for some of them. These can be found in Table 1.

Dimension-reduction

We construct a reduced representation of the SFFTN, induced by flow capacities W_{ij}^{qr} and production and demand capacities, P and D. The dimension-reduction approach considers the average dynamics by constructing an effective state, representative of the system as a whole. A set of equations for this average state is derived, taking into account the original equations and the network structure. Thus, the resulting set of equations can be directly analyzed by means of traditional Dynamical Systems tools. In the context of this problem, we regard the layer stock levels as the relevant variables, $N_q C^q y^q = \sum_{i=1}^{N_q} C^q x_i^q$. Notice that in the case of equal stock capacities, the layer stock level matches the layer average fill level. We choose to use the layer stock level as system-state variable for two reasons. First, the resulting mean-field estimator preserves the important property of flow conservation across layers. Considering different weights based on facility connectivity would lead to distortions in that property, as flows would be weighted differently depending on where they arrive to or depart from. Second, in our case study information on flow capacities at the facility level is not available, and thus it wouldn't be possible to construct an estimator based on them in the first place. However, as it will be shown below, aggregated information on flow capacities can be estimated, and thus dynamical behavior for the layer stock levels can be analyzed. By calculating the time derivatives $\dot{y}^q$, and following the typical approximations used for dimension reduction (that stock, production, demand and flow capacities are not correlated to each other, and that flow capacities and stock levels are not correlated) we obtain the set of differential equations for the layer averages y^q:

$$\begin{aligned}
\dot{y}^1 &= p\Pi(y^1) - s_{12}\Psi(y^1, y^2) - s_{13}\Psi(y^1, y^3) \\
\dot{y}^2 &= \frac{s_{12}}{\alpha_{12}}\Psi(y^1, y^2) - s_{23}\Psi(y^2, y^3) \\
\dot{y}^3 &= -d\Delta(y^3) + \frac{s_{13}}{\alpha_{12}\alpha_{23}}\Psi(y^1, y^3) + \frac{s_{23}}{\alpha_{23}}\Psi(y^2, y^3)
\end{aligned} \tag{2}$$

where:

- $p = P/C^1$ is the normalized production capacity, and $d = D/C^3$ is the normalized maximum suppliable demand.
- $s_{qr} = \sum_{i=1}^{N_q} \sum_{j=1}^{N_r} W_{ij}^{qr} / N_q C^q$ is the normalized average flow capacity from layer q to layer r.
- $\alpha_{qr} = N_r C^r / N_q C^q$ is the stock capacity ratio between layers q and r.

In the Methods section, we detail the deduction of the approximation for the general case where facilities may have different stock, production, demand and flow capacities. The approximation assumes low correlation between the system parameters and the values that the level function Π, Δ and Ψ take, similar to the assumptions in[11,13]. Numerical testing of the approximation for different connectivity patterns between gas stations and the other two layers is provided in the Supplementary Note 1, while different connectivity levels and flow capacities are considered in the Supplementary Note 2. In particular, it is worth to mention that the the approximated set in Eq. 2 works well even when stock, production, demand and flow capacities are perturbed up to a 10% of their expected value. The accuracy of the approximation increases as the interlayer connectivity and the number of nodes increase.

The approximation reduces the original set of over $3,400$ equations to only 3, allowing the use of traditional Dynamical Systems techniques to analyze the dynamics of the system in terms of global, average parameters. In turn, we change our focus of analysis from the details of each facility to the macroscopic dynamics between layers. The dimensionally reduced system captures the macroscopic behavior of the demand, without focusing on the details at the level of the facilities. By considering the layer stock level, the system's dynamics are approximated by a reduced set of equations, universal for all systems with equal stock capacity structure and average production, demand, and flow capacities. We approximate each layer independently, to account for the transportation between them.

A relevant magnitude for describing the behavior of the system is the total amount of resource stored in it, denoted as U. In terms of normalized parameters, it can be written as $U = y^1 + \alpha_{12}(y^2 + \alpha_{23} y^3) \in [0, 1 + \alpha_{12}(1 + \alpha_{23})]$, where its value is normalized by the total capacity of the first layer $N_1 C^1$ (and thus the total stock in Mgal is equal to $N_1 C^1 U$). The ranges of values for the normalized parameters can be found in Table 2.

Stable states

In resource-flow dynamics, it is usual to have a continuous range of possible stable flow levels[9], depending on the amount of resource entering or exiting the system. Thus, we look for conditions that consider stable demand or production as variable parameters. We define Π^*, Δ^*, and Ψ^*, as the stable production, demand, and flow levels. By setting $\dot{y}^q = 0$ in Eq. 2, we find the two following conditions linking them:

$$\begin{aligned} &p\Pi^* = \alpha_{12}\alpha_{23} d \Delta^* \\ &\alpha_{12}\alpha_{23} d \Delta^* \leq s_{13} + \min(s_{12}, \alpha_{12} s_{23}) \end{aligned} \tag{3}$$

The first condition requires stable production and demand levels Π^* and Δ^* to be proportional to each other. Notice that $p = P/C^1$ is the total production capacity and that $\alpha_{12}\alpha_{23} d = N_3 D / N_1 C^1$ is the total demand capacity, both in units of total stock capacity of refineries. The second condition indicates that the average demand has to be lower than the addition of the flow capacities from layer 1 to layer 3 for that demand level to be stable. For the purpose of this work, we assume that the first condition in Eq. 3 is always satisfied, meaning that the total production is equal to the total demand, and thus the stability of the system only depends on the flow capacities. The second condition from Eq. 3 is equivalent to the maximum flow theorem between the layers[28]. By considering the constraints over the stable flows imposed by this condition, we find that they are confined to a line in a 3-dimensional space (see Methods section for the full deduction of Eq. 3) for each value of the stable demand Δ^*. Thus, network structure shapes the stable state space through the maximum flow condition, limiting stable flows to those satisfying it. However, notice that the stable stock levels depend on the functions Π, Δ and Ψ being considered. Comparing these results with the findings from[11], we can see two examples of how network structure shapes the stable state spaces of the ordinary differential equations. In[11], the mutualistic interaction considered has a positive effect on each pair of species involved (i.e. it increases the number of individuals of both species). As network connectivity increases, there is a critical point above which the interaction percolates, making the system resilient to sudden reductions in the abundance of each species. In the case of resource-flow networks, the topology limits the stable flows to those satisfying the maximum flow condition[28]. Future advances in this topic could help understand further how the evolution of different systems is shaped by the intertwine between dynamics and network structures of various types.

Numerical example

While the stability of the system can be addressed in general, assessing many dynamical characteristics (as stable stock levels) requires specifying functions Π, Δ, and Ψ. However, only aggregated information is available for the SFFTN. Thus, we look to model its dynamics by considering three simple characteristics. First, according to the CEC, the production is held constant at maximum capacity, independently of the stock level of the refineries. Thus, we set $\Pi(x)$ to be approximately constant except for stock levels near $x \approx 1$, when a refinery would not have enough stock space to produce more. We consider a similar behavior for $\Delta(x)$, being constant aside from stock levels near $x \approx 0$, where a gas station would not be able to supply any demand due to the absence of resources. For the flow level $\Psi(x_1, x_2)$, we assume that it will increase as the sender x_1 has a higher stock level (more to send), or the receiver x_2 has a lower stock level (more space to receive). Figs. 2 a, b and c depict the functions $\Pi(x)$, $\Delta(x)$ and $\Psi(x_1, x_2)$ used for this work. Under these functions, the system dynamics present a smooth evolution to a stable point (see Fig. 2 d). The approximation captures well the layer stock level, while the different facilities show dispersion around it due to the differences in the flow capacities. The stable values of the layer stock levels y^q depend on the initial amount of resource saved in the system, $U(t=0)$ (Fig. 2 e). For low amounts of total resources, most of them are located at refineries, leaving the third layer empty below a certain point. The flow capacities can change the size and shape of the stable state space. For example, at a given value of $U(t=0)$, increasing the value of s_{12} reduces the stable stock level at refineries (y^1), and increases the stable stock level at gas stations (y^3). This is due to the increased flow, that moves resource to the third layer faster than it is consumed. Notice that the stable stock levels y^q are bounded between two values (different for each layer), dependent on s_{12}. Thus, the total stable resource $U(t)$ is also bounded. As s_{12} reduces, the resource is more concentrated in the first layer, leaving the third layer empty. Similar effects can be observed by changing the value of the other two normalized average flow capacities.

Impacts of SLR on the system dynamics

Next, we consider the impact of SLR on the maximum stable demand that the system would be able to sustain. We assume that in all the scenarios the total production and demand remain constant. Thus, as refineries and gas stations are removed from the system due to flooding, average capacities p and d increase to maintain constant (and equal) total production and demand. Fig. 3 a shows the average percentage changes of the parameters due to flooding, for the two RCP and the 4 time horizons considered at the 99.9 (worst case) SLR percentile. The majority of the parameters reduce their values, except for the average production capacity p and the total capacity ratio α_{23}. The biggest change occurs in the flow capacity from refineries to terminals, with a reduction of 40% (RCP 4.5) and 75% (RCP 8.5) of s_{12} (representing the pipeline average flow capacity from refineries to terminals). This is followed by a similar decrease for s_{13}, the flow capacity from refineries to gas stations directly. The value of p increases when the number of refineries reduces to keep the total production constant. α_{23} increases as proportionally more terminals are affected than gas stations. More detail on the changes of the parameters can be found in Table 3 in the Methods section.

The system is able to sustain the original demand in the time horizons 2020-2040 and 2040-2060 for all the scenarios considered. However, demand failure is observed in 2080-2100 for RCP 4.5 and 2060-2080, 2080-2100 for RCP 8.5 and 95 and 99.9 SLR percentiles (Fig. 3 b and c). This is due to two effects combined, observed in Fig. 3 b. On one hand, the flow capacities from refineries to the other facilities reduce, limiting the maximum flow that the system is able to establish. On the other hand, the reduction in the number of terminals (expressed through the decrease of α_{12} and increase of α_{23}) requires a higher average flow to and from each terminal to keep supplying the total demand. This is represented in Fig. 3 b, where we consider a phase-like diagram for the maximum stable demand constructed with the dynamics from Fig. 2 a. The diagrams show the maximum stable demand as a function of s_{12} and s_{13}, with the remaining parameters fixed at their average value for the two considered RCPs and the last two time horizons, for the worst case scenario (99.9 SLR percentile). Each white dot in the demand diagrams corresponds to the average value of the flow capacities for each of the four GCM. Flooding reduces the flow capacities, (white dots move to the lower left of each diagram). At the same time, the region with maximum stable demand below 1 increases (red region increases). Interestingly, the results are similar for RCP 4.5 within 2080-2100 and RCP 8.5 within 2060-2080, where the flow capacities are at the border of the low-demand region. For RCP 8.5 within 2080-2100, the estimated flow capacities are completely inside the low-demand region, indicating that the system is far from being able to supply the full demand.

Topological constraints on the stable demand

While the diagrams in Fig. 3 b depict the effect of coastal flooding on the maximum stable demand, they depend on the specific dynamics considered (Fig. 2 a). Inspired by the generalized modeling framework[8,9], we consider a metric that only takes into account the capacity structure of the network, and thus consider the minimum requirements over the stable demand (Eq. 3), necessary over any functions Π, Δ and Ψ. We estimate the percentage of scenarios under which the system is able to provide a given demand level. For this purpose, we take into account the ranges of values for each of the original parameters alongside the different SLR scenarios. We use Eq. 3 to measure the ability of the system to sustain a given stable demand level Δ^*, and

calculate the percentage of scenarios where the condition is satisfied. The results are presented in Fig. 3 c, for the three SLR percentiles, the last two time horizons and the two RCPs. While for RCP 4.5 within 2060-2080 there is only a slight chance of failing to supply 100% of the original demand ($\Delta^* = 1$), the percentage of scenarios unable to sustain 100% of the demand increases to 60% (for the 99.9 percentile) within 2080-2100. For RCP 8.5 the percentage is around 60% (for the 99.9 percentile) for 2060-2080, increasing to 100% for any demand over 50 of the original demand.

Production interruption under IPCC scenarios of Sea Level Rise

The previous analysis depicts the impact of permanent, long-term changes that affect the topology of a resource-flow network by modifying the size relation between layers and their flow capacities. These long-term changes may interplay with other, short-term, failure events. As an example, we consider production interruptions, that could be associated with a stoppage of supply to the refineries. We model this failure event by setting $p = 0$ in the model during a finite amount of time ΔT, ranging from half week to three weeks, and then re-establishing its original value. We initialize the system in a stable state (associated with a particular value of U), and set $p = 0$ during a time-lapse ΔT. As the demand is constant, the third layer decreases its stock level at rate d. Depending on the duration of the failure, we observe three outcomes from the production failure (Fig. 4 a). For small ΔT (Fig. 4 a, $\Delta T = 0.5$ and 1.5 weeks), the total amount of resources is reduced, but none of the layers reach near-zero stock levels. Notice how, independently of which layer reaches the lowest stock level during the failure, once the failure resumes, the stock levels reorganize based on the new value of U. For intermediate ΔT (Fig. 4 a, $\Delta T = 2$ weeks), the failure may reduce U up to a point where the $y^3 \approx 0$, even after production is restored. This is a side effect of the redistribution of resources across layers, as demonstrated in Fig. 2 e, where it is shown how at low values of U, $y^3 \approx 0$. As expected, for large ΔT, all the layers are depleted before the failure ends (Fig. 4 a, $\Delta T = 5$ weeks). Notice that when $y^3 \approx 0$, $\Delta(y^3)$ starts to decrease, and thus we observe a demand failure. As the system is initially producing at maximum capacity, when production is restored the system stabilizes in a lower level of resource, instead of going back to the original state. To increase the total resource U the system would require to have a higher production than demand. Under our assumptions, this only happens if demand fails, allowing production to accumulate in the different layers.

We analyze two aspects of production failure: the time that it takes the system to reach demand failure τ (that is, the time it takes for the third layer to reach $y^3(\tau) \approx 0$), and the average demand level during failure Q_D:

$$Q_D = \frac{1}{T}\int_0^T \Delta(y^3(t))dt \tag{4}$$

Where T is the time period under consideration. Notice that it is not required for T to be equal to the failure duration, as the aftermath can be of relevant to. T hese two metrics capture part of the dynamic aspects of the failure, moving one step forward from stable state analysis. To study the behavior of the system under this transient failure, we simulate the evolution of the system using the average values of each parameter (for each considered scenario), and initialize the stock levels y^q at stable states with different values of U. Recall that, as depicted in Fig. 2 c, stable stock levels y^q depend on the initial resource stored in the system $U(t = 0)$, and are limited by the flow capacities s_{qr}. For each coastal flooding scenario, we consider failure duration ΔT from 0.5 to 3 weeks. We use this set of simulations to measure the time to demand failure τ and the average demand level Q_D.

To study the time to demand failure τ, we consider the longest failure duration $\Delta T = 3$ weeks and measure at which time the system stops being able to supply the required demand. We use $\Delta T = 3$ weeks as all the considered settings reach failure within that time. Notice that this corresponds to the bottom right of Fig. 4 a. Fig. 4 b shows the value of τ as a function of the initial total resource in the network $U(t = 0)$. Obviously, τ increases with $U(t = 0)$ (if the system has more resources stored, it will take more time for it to get depleted). As the network is impacted by coastal flooding, we see two effects. First, for the same value of $U(t = 0)$, the value of τ is lower as we consider farther time horizons. At the same time, the change in parameters reduces the range of stable values for U, producing a smaller range of values for $U(t = 0)$, undermining the possibility of starting from a more stock full stable state. As we consider scenarios with higher levels of coastal flooding, we see a decrease of the higher τ from ≈ 3 weeks, to approximately 1.5 weeks in 2080-2100 with RCP 4.5 and the 50 SLR percentile. A similar value is found for 2060-2080 at RCP 8.5 and the 50 SLR percentile and RCP 4.5 with the 95 percentile of SLR. Once the network is unable to provide full demand, the range of $U(t = 0)$ concentrates at a single point, and $\tau \approx 0$ for that value. This can be seen in Fig. 4 b, for 2080-2100 at RCP 8.5 and 50 SLR percentile, and for the 2060-2080 at RCP 4.5 and 8.5 for the 95 SLR percentile. Comparing with Fig. 2 e, we see that as the flow capacities are reduced, the stable stock level of refineries reaches 1, and the stock level of terminals stabilizes at an intermediate value, dependent on the specific value of the flow capacities. Fuel is not able to reach the gas stations, and thus the system is essentially at demand failure.

While τ estimates how long the system will last without failing, Q_D estimates its performance during a given failure. Notice that while τ measures directly a characteristic of the production failure (when the system stops being able to supply full demand), Q_D provides an overview on the restoration of the demand as well, as it takes into account the value after the demand

has been restored. As all the considered scenarios reach failure after 3 weeks, we choose $T = 3$ weeks in Eq. 4. This way, we compare all the failure evolutions under the same time period. As demand failure depends on the value of U at the start, we average Q_D over the possible values of initial resource U. Fig. 4 c shows the values of Q_D for the different failure duration ΔT and scenarios considered. We observe a common behavior: for short failures ($\Delta T < 1$ week), $Q_D \approx 1$. Then, as ΔT increases, Q_D transitions to a linear decreasing function of ΔT. This means that for short failures the demand is not affected, and for long failures the decrease is linear in the failure duration, in accordance with Fig. 4 a. For all the scenarios considered, the total decrease in Q_D is approximately 10% at $\Delta T = 3$ weeks. When comparing Q_D as a function of ΔT for the different SLR scenarios, we observe very similar curves, with a lower Q_D at a given ΔT as we consider further time horizons. The curve only changes slightly for system capable of providing full demand, with the highest difference around 5% for $\Delta T = 3$ weeks. For failed systems, Q_D is noticeable below 1 for $\Delta T = 0.5$ week, as the demand is heavily impacted by the coastal flooding.

Limitations and advantages of dimension-reduction for sociotechnical systems

We have presented on the application of dimensional reduction to resource flow systems, particularly exemplified by the transportation of fuel in the San Francisco Bay Area. The approximation aggregates the facilities based on their stock capacities, producing system-level variables that capture layer-level dynamics. It allows studying a very complex networked system, including thousands of different facilities from an aggregated perspective, even with very limited information. As it is discussed in the Supplementary Note 1, the approximation still works well under random perturbation of the different types of parameters. However, by aggregating the system we ignore internal correlations that may exist in it (for example, correlations between production and flow capacities). Systems with significant correlations between their parameters (i.e. stock, production and demand capacities) might not be well captured by this aggregated approximations. The Supplementary Note 1 includes testing of the approximation for different in degrees of gas stations, varying to how many terminals and refineries they connect to. The test shows that as long as gas stations connect to more than 10 terminals, the approximation has less than 5% error. Even more, the approximation still works well under small variations of the parameters (while still maintaining the same average value).

From the perspective of the applications to real systems, we consider that dimension-reduction supposes two contributions to the analysis of large, interconnected socio-technical systems. First, it allows providing estimates of the impact of failures even with very limited information. Of course, in the case of trying to precisely estimate the impact of extreme events on a particular network, researchers should look for the most detailed information possible. Nevertheless, the procedure discussed here is independent on the specific functional forms considered. Second, dimensional reduction can be extremely useful as we consider systems of systems, where each system is already complex on its own. Simplifying the subsystems can serve as starting point for assessing the behavior of a system of systems, by including them from an analytically tractable point of view, and assess their interactions as a whole.

Discussion

We presented an analysis of the demand levels that the San Francisco Fuel Transportation Network is able to satisfy under different coastal flooding scenarios. We focused on the demand stability under the perturbations induced by coastal flooding, and its dynamic behavior under a production failure. We approximate the system's dynamics by reducing its dimension, focusing on the aggregated flow between refineries, terminals and gas stations. By working with the dynamical representation of the system, changes in network topology can be directly related to its role as resource supplier, helping to reduce the gap between traditional network measures (like number of connected components or global efficiency) and realistic policies (like demand rationing), more accessible to decision-makers.

By considering layer dynamics through the dimension-reduction approach, we find that the space of stable macroscopic flows is constrained by a relationship equivalent to the maximum flow theorem between layers. This result adds up to the findings for mutualistic interactions in[11], which demonstrate how the stability of the system is connected to the percolation of the mutualistic interaction through the network, allowing the system to recover from reductions in the abundance of each species. Further analysis on other network structures can expand the understanding on how network topology shapes the dynamics of networked ordinary differential equations.

In the case study considered here, the assumptions used for the approximation are reasonable as the pipeline system and road networks allows transporting fuel essentially from any facility to any other, while at the same time we do not have access to greater detail on the flows between facilities. However, in more complex structures, with higher levels of heterogeneity, other system-state variables may be preferred. The goal of the dimension-reduction framework is to map the high-dimensional dynamics to a smaller set of relevant system variables, which may be different depending on the problem, and thus they should be adjusted depending on the case under consideration. For example, the state-variable considered here preserves flow properties typical from resource-flow systems, while the estimator used in[11] is specially designed to put emphasis on hubs, which are crucial for percolation of interactions.

Our results indicate that the structure of the San Francisco Fuel Transportation Network would be able to sustain the current demand during the period 2020-2060. Yet, the current structure will likely start being affected after that period, specially under high levels of greenhouse gas emissions. Through failure simulation, we find that the maximum survival time without production decreases from three weeks to one and a half even in the best-case scenario (for a three weeks production stoppage). However, as only very limited information is available on the network dynamics, these values should be considered as broad estimations. It would be interesting to consider the dimension-reduction approach in other transportation networks, where more information is available, and the effect of differences on production, stock, demand and flow capacities can be compared with data.

We show that the dimension-reduction approach can help understand better the dynamics of lifeline systems, by constructing analytically tractable representations that capture their macroscopic behavior. While these simplifications average the details on finer scales, they allow studying the effect of changes in the infrastructure from a system level perspective. In future analysis, it would be interesting to explore through the dimension-reduction approach how different lifeline infrastructures interact with each other, forming systems of systems. The reduction can help by simplifying the dynamics of each sub-system, while keeping tract of their interactions. Steps in this direction have already been done in the context of Ecology[12], by considering the interaction between network communities. Increasing our understanding of how dynamics of interconnected lifeline infrastructure are affected by climate extreme events is crucial for preparation for the changes our world is currently facing.

Methods

The San Francisco Fuel Transportation Network

The network topology of the SFFTN has been analyzed in a previous project by He et al.[21]. The spatial elements conforming the network were obtained from multiple sources. Location of refineries and terminals was provided by the U.S. Energy Information Administration. The location of gas stations was obtained through Google Places. Pipeline structure was obtained through the U.S. National Pipeline Mapping, and roads were downloaded from OpenStreetMaps[29]. To connect pipelines and roads with the three different facilities, the nearest node in each transportation network was connected to each facility (only roads in the case of gas stations). This provides the spatial representation necessary to assess the impact of coastal flooding.

Layered dimension reduction

Following previous work from Gao et al.[11] we construct an approximation that captures the average behavior of the different layers in the transportation network. The dimension-reduction approach was originally developed in the context of the Barzel-Barabasi equation,

$$\dot{x}_i = F(x_i) + \sum_{i=1}^{N} A_{ij} G(x_i, x_j) \tag{5}$$

that considers an homogeneous interaction across all the elements of the system. In the Eq. 5, F and G represent self and pair interactions, and A_{ij} is the adjacency matrix associated to the interaction graph. Effective variables are constructed through weighting each variable based on their connectivity in the network. However, in the context of resource-flow networks, interactions have to take into account incoming and outgoing flow to adjacent nodes. Thus, an extension of the original approach is necessary. From the point of view of system stability analysis, dimension-reduction operates by constructing a single variable representing the system's global state. This variable is a function of the constituents of the systems. In[11], the system-level variable is constructed by weighting each variable based on its connectivity. This leads to a system-average that puts emphasis on more connected nodes. While this makes sense for mutualistic interactions, it is not the only option possible. For the purpose of this work, we will consider that the importance of a node is dependent on their stock capacity C^q, which is a property of the facility instead of its connectivity. While weighting each node by its degree (or strength, equivalent to its total flow capacity in the context of resource-flow) puts the focus on the node that has the highest connectivity, weighting by node's stock capacity we preserve the connection between our system variables and the total amount of resource stored in the system (essential in the context of flow of resources). At the same time, if we wanted to weight each node based on their connectivity, it would be necessary to distinguish between incoming and outgoing flow capacities. This would lead to an asymmetric estimator, which considers each layer differently depending on which side we are looking at. By weighting by the node's stock capacity, we obtain a symmetric weighting, independent of the flow direction.

In the dynamical description of the transportation network, the state of each facility is described by x_i^q, the stock level of node i in layer q. Here, we derive the equations departing from a slightly more general point of view than the one described in section . We consider that every facility has its own stock capacity C_i^q, production capacity P_i (in refineries) and demand capacity D_i (in gas stations). We derive the equations with more generality looking to make the proposed approximation more

clear, while for the application discussed in the Results we simplify by considering every capacity equal due to the lack detail in the data. The goal is to obtain a set of equations capturing the dynamics of the fuel stored at each of the three facility layers. The stock level of facility i in layer q is represented by x_i^q. The evolution of the variables x_i^q is described by the set of ordinary differential equations:

$$\begin{aligned}
C_i^1 \dot{x}_i^1 &= P_i \Pi(x_i^1) - \sum_{j=1}^{N_2} W_{ij}^{12} \Psi(x_i^1, x_j^2) - \sum_{j=1}^{N_3} W_{ij}^{13} \Psi(x_i^1, x_j^3) \\
C_i^2 \dot{x}_i^2 &= \sum_{j=1}^{N_1} W_{ji}^{12} \Psi(x_j^1, x_i^2) - \sum_{j=1}^{N_3} W_{ij}^{23} \Psi(x_i^2, x_j^3) \\
C_i^3 \dot{x}_i^3 &= -D_i \Delta(x_i^3) + \sum_{j=1}^{N_1} W_{ji}^{13} \Psi(x_j^1, x_i^3) + \sum_{j=1}^{N_2} W_{ji}^{23} \Psi(x_j^2, x_i^3)
\end{aligned} \tag{6}$$

where the C_i^q is the stock capacity of facilities in layer q, P_i the production capacity of refinery i in layer 1, D_i the demand capacity of gas station i in layer 3 and W_{ij}^{qr} is the flow capacity between node i in layer q and node j in layer r. The total amount of resource in layer q is $\sum_{i=1}^{N_q} C_i^q x_i^q$, and thus the stock level of layer q is $y^q = \frac{1}{N_q C^q} \sum_{i=1}^{N_q} C_i^q x_i^q$, where $C^q = \sum_{i=1}^{N_q} C_i^q$. To obtain a differential equation for the layer stock level y^q, we take the derivative and approximate Eq. 6. Then, we have the three equations:

$$\begin{aligned}
N_1 C^1 \dot{y}^1 &= \sum_{i=1}^{N_1} C_i^1 \dot{x}_i^1 = \sum_{i=1}^{N_1} \left\{ P_i \Pi(x_i^1) - \sum_{j=1}^{N_2} W_{ij}^{12} \Psi(x_i^1, x_j^2) - \sum_{j=1}^{N_3} W_{ij}^{13} \Psi(x_i^1, x_j^3) \right\} \\
N_2 C^2 \dot{y}^2 &= \sum_{i=1}^{N_2} C_i^2 \dot{x}_i^2 = \sum_{i=1}^{N_2} \left\{ \sum_{j=1}^{N_1} W_{ji}^{12} \Psi(x_j^1, x_i^2) - \sum_{j=1}^{N_3} W_{ij}^{23} \Psi(x_i^2, x_j^3) \right\} \\
N_3 C^3 \dot{y}^3 &= \sum_{i=1}^{N_3} C_i^3 \dot{x}_i^3 = \sum_{i=1}^{N_3} \left\{ -D_i \Delta(x_i^3) + \sum_{j=1}^{N_1} W_{ji}^{13} \Psi(x_j^1, x_i^3) + \sum_{j=1}^{N_2} W_{ji}^{23} \Psi(x_j^2, x_i^3) \right\}
\end{aligned} \tag{7}$$

Following the common steps of the mean-field approximation, we assume that the correlation between stock, production and flow capacities, and the values of the functions $\Pi(x)$, $\Delta(x)$ and $\Psi(x,y)$ are low. Then, we can approximate the average of the products with the product of the averages. For the production term, we have:

$$\frac{1}{N_1 C^1} \sum_{i=1}^{N_1} P_i \Pi(x_i^1) \approx \frac{1}{C^1} \left(\frac{1}{N_1} \sum_{i=1}^{N_1} P_i \right) \left(\frac{1}{N_1} \sum_{i=1}^{N_1} \Pi(x_i^1) \right) \approx \frac{P}{C^1} \left(\frac{1}{N_1} \sum_{i=1}^{N_1} \Pi(x_i^1) \right) \tag{8}$$

To link the average of functions $\Pi(x_i^1)$ with the layer stock level y^1, we recall the results from[13], where the authors propose to make a polynomial decomposition of the functions, and subsequently repeat the approximation over the expansion coefficients. In that case, we have (to first order, the three dots represent the next terms in the expansion):

$$\begin{aligned}
\frac{1}{N_1} \sum_{i=1}^{N_1} \Pi(x_i^1) &\approx \frac{1}{N_1} \sum_{i=1}^{N_1} \Pi(0) + \Pi'(0) x_i^1 + \dots \\
&= \Pi(0) + \frac{1}{N_1} \Pi'(0) \sum_{i=1}^{N_1} \frac{C_i^1}{C_i^1} x_i^1 + \dots \\
&\approx \Pi(0) + \Pi'(0) \left(\sum_{i=1}^{N_1} \frac{C^1}{N_1 C_i^1} \right) y^1 + \dots \\
&\approx \tilde{\Pi}(y^1)
\end{aligned} \tag{9}$$

Where in the third line we approximated $\sum_{i=1}^{N_1} x_i^1 \approx \sum_{i=1}^{N_1} y^1 C^1 / C_i$. Thus, the approximation leads to a layer production function $\sum_{i=1}^{N_1} P_i \Pi(x_i^1)/N_1 \approx P \tilde{\Pi}(y^1)$, where P is the refinery's average production capacity and $\tilde{\Pi}(y^1)$, which is an average of the

production levels, weighted by the inverse of the stock capacity of each layer. To first order, and under the assumption of low correlation between the polynomial expansion coefficients and the stock levels, the coefficient involving the capacities is $C^1 \sum_{i=1}^{N_1} 1/C_i^1$. This re-scaling accounts for the variability of the capacities across facilities (and thus, for the different scales of each production function). In the context of our work, where we consider that all the refineries have the same stock capacity, the function $\tilde{\Pi}$ matches exactly the function Π. In general, the quality of the approximation should be tested for other functions Π and stock capacities based on the case under study. The derivation discussed is equivalent to the one for $\sum_{i=1}^{N_3} D_i \Delta(x_i^3)/N_3 \approx D\tilde{\Delta}(y^3)$.

For the flow terms, we follow a similar procedure, with the minor difference that summation is done over the two layers:

$$\begin{aligned}
\frac{1}{N_q}\sum_{i=1}^{N_q}\sum_{j=1}^{N^r} W_{ij}^{qr}\Psi(x_i^q,x_j^r) &= \frac{N_r}{N_q N_r}\sum_{i=1}^{N_q}\sum_{j=1}^{N^r} W_{ij}^{qr}\Psi(x_i^q,x_j^r) \\
&\approx N_r\left(\frac{1}{N_q N_r}\sum_{i=1}^{N_q}\sum_{j=1}^{N_r} W_{ij}^{qr}\right)\left(\frac{1}{N_q N_r}\sum_{i=1}^{N_q}\sum_{j=1}^{N_r}\Psi(x_i^q,x_j^r)\right) \\
&\approx \frac{W^{qr}}{N_q}\sum_{i=1}^{N_q}\sum_{j=1}^{N_r}\frac{1}{N^q N^r}\Psi(x_i^q,x_j^r) \\
&\approx \frac{W^{qr}}{N_q}\tilde{\Psi}(y^q,y^r)
\end{aligned} \tag{10}$$

Where $W^{qr} = \sum_{i=1}^{N_q}\sum_{j=1}^{N_r} W_{ij}^{qr}$ is the total flow capacity between layers q and r. To approximate function Ψ and obtain function $\tilde{\Psi}$, the approximation steps are as follows (again to first order, with dots representing higher orders in the Taylor expansion):

$$\begin{aligned}
\frac{1}{N_q}\frac{1}{N_r}\Psi(x_i^q,x_j^r) &\approx \frac{1}{N_1 N_2}\sum_{i=1}^{N_q}\sum_{j=1}^{N_r}\Psi(0,0)+\Psi'_q(0,0)x_i^q+\Psi'_r(0,0)x_j^r+\dots \\
&= \Psi(0,0)+\frac{1}{N_q}\sum_{i=1}^{N_q}\Psi'_q(0,0)x_i^q+\frac{1}{N_r}\sum_{j=1}^{N_r}\Psi'_r(0,0)x_j^r+\dots \\
&= \Psi(0,0)+\frac{1}{N_q}\sum_{i=1}^{N_q}\Psi'_q(0,0)\frac{C_i^q}{C_i^q}x_i^q+\frac{1}{N_r}\sum_{j=1}^{N_r}\Psi'_r(0,0)\frac{C_j^r}{C_j^r}x_j^r+\dots \\
&= \Psi(0,0)+\frac{y^q}{N_q}\sum_{i=1}^{N_q}\frac{C^q\Psi'_q(0,0)}{C_i^q}+\frac{y^r}{N_r}\sum_{j=1}^{N_r}\frac{C^r\Psi'_r(0,0)}{C_j^r}+\dots \\
&\approx \tilde{\Psi}(y^q,y^r)
\end{aligned} \tag{11}$$

In this case, the approximation yields the term $W^{qr}\tilde{\Psi}(y^q,y^r)/N_q$. This term includes function $\tilde{\Psi}$, the average flow level from layer q to layer r, and the average total flow capacity of a facility in layer q to the whole layer r. For the case in which we consider incoming flow instead of outgoing, the expression slightly changes, as we are summing over layer r instead of over layer q. This leads to the expression $W^{qr}\tilde{\Psi}(y^q,y^r)/N_r$, and thus the global flow level is multiplied by the average (in)flow capacity perceived by nodes in layer r, considering all nodes in layer q. As in the previous case, when we consider all the nodes in the same layer to have the same stock capacity, function $\tilde{\Psi}$ matches Ψ. Thus, we obtain the final set of equations:

$$\begin{aligned}
C^1\dot{y}^1 &\approx P\tilde{\Pi}(y^1)-\frac{W^{12}}{N_1}\tilde{\Psi}(y^1,y^2)-\frac{W^{13}}{N_1}\tilde{\Psi}(y^1,y^3) \\
C^2\dot{y}^2 &\approx \frac{W^{12}}{N_2}\tilde{\Psi}(y^1,y^2)-\frac{W^{13}}{N_2}\tilde{\Psi}(y^2,y^3) \\
C^3\dot{y}^3 &\approx -D\tilde{\Delta}(y^3)+\frac{W^{13}}{N_3}\tilde{\Psi}(y^1,y^3)+\frac{W^{23}}{N_3}\tilde{\Psi}(y^2,y^3)
\end{aligned} \tag{12}$$

where we recall that, in the case of equal stock capacities ($C_i^q = C^q$), $\tilde{\Pi} = \Pi$, $\tilde{\Delta} = \Delta$ and $\tilde{\Psi} = \Psi$. For the rest of the Methods section, we assume that $C_i^q = C^q$ and thus $\tilde{\Pi} = \Pi$, $\tilde{\Delta} = \Delta$ and $\tilde{\Psi} = \Psi$.

To take this set of equations to a more compact form involving less parameters, we divide each equation by the corresponding stock capacity, and rename the combined parameters. This leads to:

$$\begin{aligned}
\dot{y}^1 &= p\Pi(y^1) - s_{12}\Psi(y^1,y^2) - s_{13}\Psi(y^1,y^3) \\
\dot{y}^2 &= \frac{s_{12}}{\alpha_{12}}\Psi(y^1,y^2) - s_{23}\Psi(y^2,y^3) \\
\dot{y}^3 &= -d\Delta(y^3) + \frac{s_{13}}{\alpha_{12}\alpha_{23}}\Psi(y^1,y^3) + \frac{s_{23}}{\alpha_{23}}\Psi(y^2,y^3)
\end{aligned} \tag{13}$$

where:

- $p = P/C^1$ is the normalized production capacity, and $d = D/C^3$ is the normalized maximum suppliable demand (which we call demand capacitiy).
- $s_{qr} = \sum_{i=1}^{N_q}\sum_{j=1}^{N_r} W_{ij}^{qr}/N_qC^q$ is the normalized average flow capacity from layer q to layer r.
- $\alpha_{qr} = N_rC^r/N_qC^q$ is the stock capacity ratio between layers q and r.

The quotient between average normalized flow capacities and total capacity ratios represents the different perspective on the average depending on the layer: while s_{12} can be seen as the average *outflow* capacity of a refinery, $s_{12}/\alpha_{12} = W^{12}/N_2C^2$, the normalized average *inflow* capacity at terminals.

The (normalized) total resource stored in the system is $U = y^1 + \alpha_{12}(y^2 + \alpha_{23}y^3)$, while N_1C^1U is the total resource stored in the original units. Thanks to the internal balance of flows within the system, we have:

$$\dot{U} = p\Pi(y^1) - \alpha_{12}\alpha_{23}\Delta(y^3) \tag{14}$$

Which represents the global balance of resource in the whole system. Notice that the balance of resource stops changing ($\dot{U} = 0$) when production and demand balance each other, and that the change in time of U does not depend on the stock level of the intermediate layer.

Stable state

To identify the stable state we set $y^q = 0$ in Eq. 13, and identify the conditions for stability. As we haven't precised functional forms for Π, Δ and Ψ yet, we focus on the conditions over these functions first. If we call y^{q*} the values of the (average) stable stock levels at layer q, and we define $\Pi(y^{1*}) = \Pi^*$, $\Delta(y^{2*}) = \Delta^*$ and $\Psi(y^{q*}, y^{r*}) = \Psi^*_{qr}$, then:

$$\begin{aligned}
p\Pi^* &= s_{12}\Psi^*_{12} + s_{13}\Psi^*_{13} \\
s_{12}\Psi^*_{12} &= \alpha_{12}s_{23}\Psi^*_{23} \\
\alpha_{12}\alpha_{23}d\Delta^* &= s_{13}\Psi^*_{13} + \alpha_{12}s_{23}\Psi^*_{23}
\end{aligned} \tag{15}$$

The solution to these equations only exists if the production and demand are balanced,

$$p\Pi^* = \alpha_{12}\alpha_{23}\Delta^* \tag{16}$$

Under this condition, the stable flows are define by Δ^* (or equivalently by Π^*).

$$\begin{pmatrix} \Psi^*_{13} \\ \Psi^*_{23} \end{pmatrix} = \begin{pmatrix} \frac{\alpha_{12}\alpha_{23}d}{s_{13}}\Delta^* \\ 0 \end{pmatrix} + \Psi^*_{12}\begin{pmatrix} -\frac{s_{12}}{s_{13}} \\ \frac{s_{12}}{\alpha_{12}s_{23}} \end{pmatrix} \tag{17}$$

We can see that all the stable flows are located within a line in the 3-dimensional space of flows for a fixed value of Δ^*. This ambiguity comes from the existence of two possible paths through which the flow can go. As total flow balance is the only condition for stability, many internal flows are possible. Notice that the range of values for Ψ^*_{12} is dependent on the different capacities and the demand level Δ^*. As each flow level Ψ^*_{qr} is constrained to be between 0 and 1, we obtain the constraint for Ψ^*_{12}:

$$\max(0, \frac{\alpha_{12}\alpha_{23}d\Delta^* - s_{13}}{s_{12}}) \leq \Psi^*_{12} \leq \min(1, \frac{\alpha_{12}s_{23}}{s_{12}}, \frac{\alpha_{12}\alpha_{23}d\Delta^*}{s_{12}}) \tag{18}$$

We can see that increasing Δ^* moves the lower range up, and increasing the flow capacity s_{12} moves the upper limit down. If we look for the border condition at which there is only a single possible value for the stable flow (and thus maximum and minimum in Eq. 18 are equal), we find the requirement:

$$\alpha_{12}\alpha_{23}d \leq s_{13} + \min(s_{12}, \alpha_{12}s_{23}) \tag{19}$$

This equation is equivalent to the max-flow theorem condition between the three considered layers. In this case, the total demand $\alpha_{12}\alpha_{23}d$ is equal to the sum of the flow capacities of the direct path from refineries to gas stations, s_{13}, and the long path from refineries to terminals, and terminals to refineries, $\min(s_{12}, \alpha_{12}s_{23})$. Comparing these result with the findings from[11], we can see two examples of how network structure shapes the stable state spaces of the differential equations. In[11], the mutualistic interaction considered has a positive effect on the pair of species involved (i.e. it increases the number of individuals of both species). The dimension-reduction captures the connectivity of the network in a single coefficient, and there is a critical point above which the mutualistic interaction percolates, making the system resilient to sudden reductions in the abundance of each species. In the context of resource-flow, the dimension-reduction captures the maximum flow condition limiting the stable flows[28].

Network capacities

Precise information on production, flow and demand capacities (P, W_{ij}^{qr} and D in Eq. 1) is not openly available. However, CEC provides total production for Northern California and average daily number of trucks[30]. We use 97.5 Mgal as a reasonable estimation of the total production capacity N_1P at the five refineries in Northern California. To estimate the demand capacity, we consider its average value as N_1P/N_3, the total production divided the number of refineries. This equates to the assumption that, on average, the system is stable (total production is equal to total demand). To obtain an estimation of the average stock capacity C^1 of the refineries, we consider the maximum total stock reported by Northern California at the refineries, provided by CEC. The maximum total stock observed is equal to 191 Mgal, or 38.2 Mgal on average per refinery. To explore a wide range of values, we consider $C^1 \in [38.2, 57.3]$ Mgal. For the terminal's stock capacity C^2, we consider the average of the stock capacities provided by Kinder Morgan[31], equal to 31.1 Mgal, and consider the range $C^2 \in [31.1, 62.2]$ Mgal. For the gas stations stock capacity, we consider a single value of $C^3 = 0.035$ Mgal, based on the information publicly provided by U.S. Oil Spill Prevention organization.

Direct estimation of individual flow capacities would require knowing policies regarding the number of trucks that a each facility can contact. However, under the dimension-reduction approximation, we can provide estimates for the total flow capacities W^{12}, W^{13} and W^{23}. According to CEC, there are approximately $5,000$ tanker truck trips per day. We assume all them occur between terminals and gas stations. We consider that the storage capacity of a tanker truck ranges between 3 and 7 thousands of gallons. Then, we consider the range for the total flow capacity between terminals and gas stations, $W^{12} \in [105, 245]$ Mgal week^{-1}. Flow from refineries to gas stations directly is also possible, while we assume it is comparatively smaller as in general it would be more costly. Thus, we consider a smaller range $W^{13} \in [21, 81]$ Mgal week^{-1}. For the pipeline flow capacity between refineries and terminals, we calculate the minimal cut to separate all the refineries from all the terminals, finding it would require to remove 5 independent segments of pipeline in the original (unperturbed) network. We consider the flow capacity of a single pipeline to be between 2 and 4 millions of gallons per day, and thus we take as range for the weekly total flow capacity $W^{12} \in [70, 140]$ Mgal week^{-1}.

Sea level rise and coastal flooding

By using sea level and climate projections between 2020 and 2100 from California's Fourth Climate Change Assessment[32] flood inundation time series maps for two Representative Concentration Pathways (RCPs) and four general climate or earth system models (GCMs), three probabilistic percentile estimates of SLR were created for a previous project[21,23]. The four GCM are CanESM2, MIROC5, CNRM-CM5 and HadGEM2-ES, corresponding to the CMIP5 suite of models[25]. The two RCPs considered are 4.5 and 8.5, representing a mild and a high level of greenhouse gas emissions. The four GCM are mathematical models that represent physical processes in the atmosphere, ocean, cryosphere, and land surface. The three probabilistic percentile estimates of SLR correspond to the 50, 95 and 99.9 estimates of SLR for a given time horizons and RCP. The SLR estimates are used as input for the 3Di hydrodynamic model[26], taking into account the elevation of the region considered and the tidal movement. The hydrodynamic model outputs the water column at $50m$ spatial resolution produced by tidal movement at each point of space during a high sea level event (i.e. a 72-hour storm event with the highest sea level at a given scenario) for each of the scenarios considered (corresponding to a combination of SLR percentile, GCM, RCP and time horizon). A detailed description of the modeling process is well documented in reference[23] under Appendix A. For the purpose of flooding impact analysis, we considered that a node was failed if the water height at its location was $15cm$ or higher, based on information provided by the fuel companies of the region.

Impact of coastal flooding

By overlaying flooding maps and network spatial representation, we identified failed nodes, removed them, and recalculated every aggregated parameter for each flooding scenario. We consider that stock and flow capacities are not affected by flooding, and thus changes in the parameters are due solely to changes in network structure. The changes in network structure are captured by the number of facilities of each type, the minimal pipeline cut to separate refineries from terminals, and the fraction of gas stations accessible from the average refinery and terminal through the road network, as explained below. A range of values for each one of the magnitudes is provided in Table 3 to provide an idea of the impact of SLR.

Total stock capacity ratios change solely due to changes in the number of nodes of each type, as stock capacities are considered fixed. For the pipeline flow capacities (associated with parameters W^{12} and s_{12}), we calculate the minimal cut between refineries and terminals under each flooding scenario, and consider as aggregated flow capacity the minimum cut times the flow capacity of a typical product pipeline. Minimum cut is reported in Table 3.

To estimate the reduction in flow capacity from terminals to gas stations (done by truck), we calculate the number of accessible gas stations for each terminal (through the road network). If the average terminal has fN_3 gas stations accessible under a given flooding scenario ($0 < f < 1$), then we estimate the new total flow capacity $W^{23\,\prime} = fW^{23}$ (with W^{23} being the original unperturbed flow capacity from terminals to gas stations). An equivalent calculation is done for the flow capacity from refineries to gas stations.

Data Availability

The original network was constructed with privacy-protected information from the fuel companies involved in fuel transportation and thus cannot be shared. The flooding maps and results from the simulations used to make the plots are available at github.com/humnetlab/sfftn-dr. All other data can be made available on reasonable request.

Code Availability

Simulations are based on ODE solver package deSolve (cran.r-project.org/web/packages/deSolve). The code used for analysis the simulations can be found at github.com/humnetlab/sfftn-dr.

Acknowledgements

A.S., A.G. and M.G. acknowledge the support of the US DoD SERDP under grant **Networked Infrastructures under Compound Extremes (NICE)** (RC20-1183), and J.R. and M.G. acknowledge the support of C3.ai under grant **Multiscale analysis for Improved Risk Assessment of Wildfires facilitated by Data and Computation**.

Author contributions statement

A.S., A.G. and M.G. conceived the project. Y.H. and J.R. reconstructed the original network and coastal flooding maps. A.S. did the analytical calculations, dynamical simulations and scenario analysis. A.S. and M.G. were the lead writers of the manuscript. All authors read and revised the manuscript.

Competing interests

The authors declare no competing interests.

References

1. Liu, X. *et al.* Network resilience. *Phys. Reports* **971**, 1–108 (2022).
2. Bhatia, U. *et al.* Aviation transportation, cyber threats, and network-of-networks: Modeling perspectives for translating theory to practice. In *2018 IEEE International Symposium on Technologies for Homeland Security (HST)*, 1–7 (IEEE, 2018).
3. Manyena, S. B. The concept of resilience revisited. *Disasters* **30**, 434–450 (2006).
4. Artime, O. *et al.* Robustness and resilience of complex networks. *Nat. Rev. Phys.* 1–18 (2024).
5. Kumar, P. Climate change and cities: challenges ahead (2021).
6. Jaroszweski, D., Chapman, L. & Petts, J. Assessing the potential impact of climate change on transportation: the need for an interdisciplinary approach. *J. Transp. Geogr.* **18**, 331–335 (2010).

7. Lee, H. *et al.* Climate change 2023: Synthesis report. contribution of working groups i, ii and iii to the sixth assessment report of the intergovernmental panel on climate change. (2023).
8. Awender, S., Wackerbauer, R. & Breed, G. A. Combining generalized modeling and specific modeling in the analysis of ecological networks. *Chaos: An Interdiscip. J. Nonlinear Sci.* **33** (2023).
9. Demirel, G., MacCarthy, B. L., Ritterskamp, D., Champneys, A. R. & Gross, T. Identifying dynamical instabilities in supply networks using generalized modeling. *J. Oper. Manag.* **65**, 136–159 (2019).
10. Yadav, N., Chatterjee, S. & Ganguly, A. R. Resilience of urban transport network-of-networks under intense flood hazards exacerbated by targeted attacks. *Sci. reports* **10**, 10350 (2020).
11. Gao, J., Barzel, B. & Barabási, A.-L. Universal resilience patterns in complex networks. *Nature* **530**, 307–312 (2016).
12. Ma, C., Korniss, G., Szymanski, B. K. & Gao, J. Generalized dimension reduction approach for heterogeneous networked systems with time-delay. *arXiv preprint arXiv:2308.11666* (2023).
13. Tu, C., D'Odorico, P. & Suweis, S. Dimensionality reduction of complex dynamical systems. *Iscience* **24** (2021).
14. Thibeault, V., St-Onge, G., Dubé, L. J. & Desrosiers, P. Threefold way to the dimension reduction of dynamics on networks: an application to synchronization. *Phys. Rev. Res.* **2**, 043215 (2020).
15. Bressan, A., Čanić, S., Garavello, M., Herty, M. & Piccoli, B. Flows on networks: recent results and perspectives. *EMS Surv. Math. Sci.* **1**, 47–111 (2014).
16. Dominguez, R., Framinan, J. M. & Cannella, S. Serial vs. divergent supply chain networks: a comparative analysis of the bullwhip effect. *Int. J. Prod. Res.* **52**, 2194–2210 (2014).
17. Pardo-Araujo, M., García-García, D., Alonso, D. & Bartumeus, F. Epidemic thresholds and human mobility. *Sci. reports* **13**, 11409 (2023).
18. Meng, F., Fu, G., Farmani, R., Sweetapple, C. & Butler, D. Topological attributes of network resilience: A study in water distribution systems. *Water research* **143**, 376–386 (2018).
19. Kulkarni, S., Dave, R., Bhatia, U. & Kumar, R. Tracing spatiotemporal changes in agricultural and non-agricultural trade networks of india. *Plos one* **18**, e0286725 (2023).
20. Hinkel, J. *et al.* Sea-level rise scenarios and coastal risk management. *Nat. Clim. Chang.* **5**, 188–190 (2015).
21. He, Y., Lindbergh, S., Ju, Y., Gonzalez, M. & Radke, J. Towards resilient critical infrastructures: Understanding the impact of coastal flooding on the fuel transportation network in the san francisco bay. *ISPRS Int. J. Geo-Information* **10**, 573 (2021).
22. Yü, J.-Z., Cai, C. & Gao, J. Bullwhip effect of supply networks: Joint impact of network structure and market demand. *arXiv preprint arXiv:2208.04459* (2022).
23. Radke, J. D., Biging, G. S., Roberts, K. H., Schmidt-Poolman, M. & University of California, B. C. f. C. R. M. *Assessing Extreme Weather-related Vulnerability and Identifying Resilience Options for California's Interdependent Transportation Fuel Sector: A Report for California's Fourth Climate Change Assessment* (California Energy Commission, 2018).
24. Van Vuuren, D. P. *et al.* The representative concentration pathways: an overview. *Clim. change* **109**, 5–31 (2011).
25. Taylor, K. E., Stouffer, R. J. & Meehl, G. A. An overview of cmip5 and the experiment design. *Bull. Am. meteorological Soc.* **93**, 485–498 (2012).
26. Stelling, G. S. Quadtree flood simulations with sub-grid digital elevation models. In *Proceedings of the Institution of Civil Engineers-Water Management*, vol. 165, 567–580 (Thomas Telford Ltd, 2012).
27. Barzel, B. & Barabási, A.-L. Universality in network dynamics. *Nat. physics* **9**, 673–681 (2013).
28. Goldberg, A. V. A new max-flow algorithm. (1985).
29. Map, O. S. Open street map. *Online: https://www. openstreetmap. org. Search* (2014).
30. Commision, C. E. Weekly fuel watch (2023). Accessed: July 2023.
31. Morgan, K. Pacific operations (2019). Accessed: July 2023.
32. Cayan, D., Kalansky, J., Iacobellis, S. & Pierce, D. Creating probabilistic sea level rise projections to support the 4th california climate assessment. *Environ. Sci* **17** (2016).

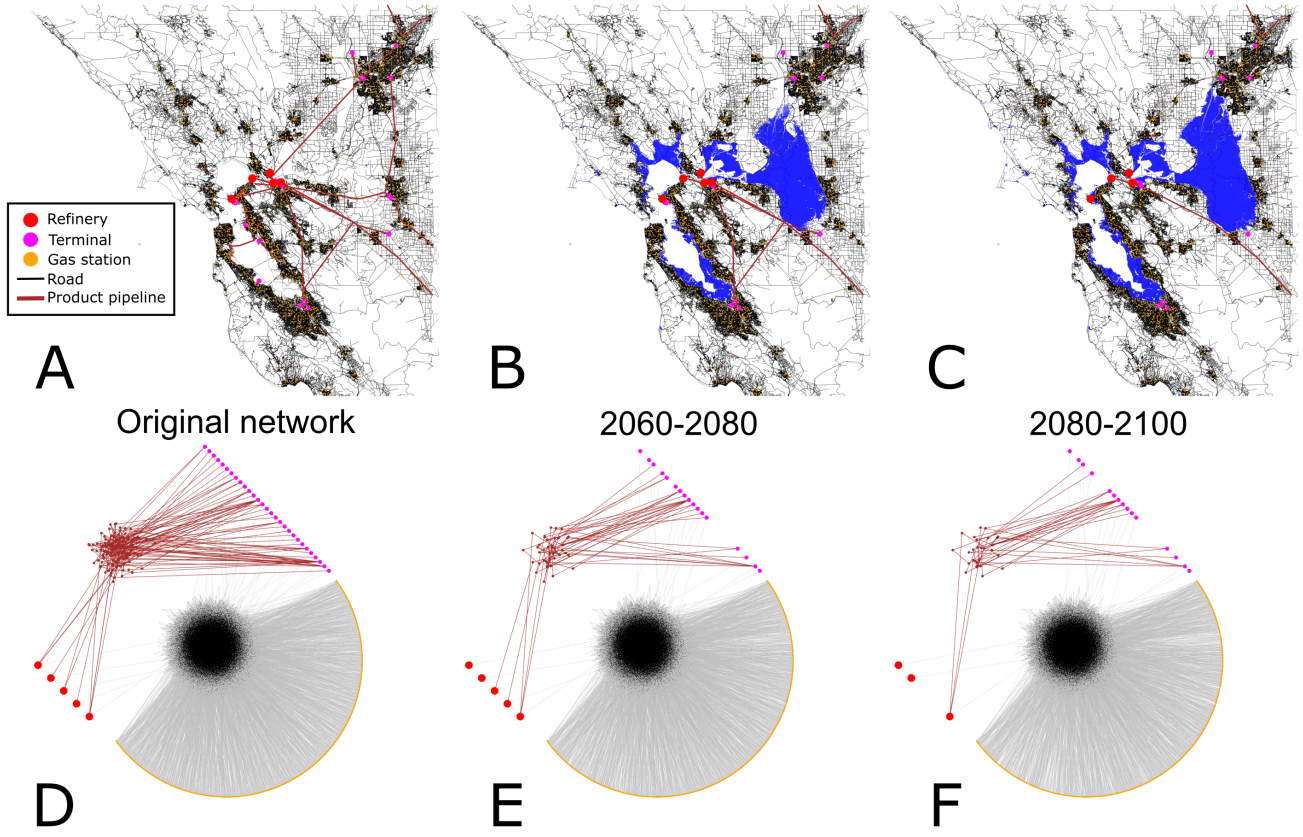

Figure 1. San Francisco Bay Area fuel transportation network, under different sea level rise scenarios. The transportation network consists of three layers, linking facilities (refineries, terminals and gas stations), through transportation means (roads and product pipelines). a: Original network, represented in space. b and c: Spatial representation of the network at RCP (Representative Concentration Pathways) 8.5 and 99.9 SLR (Sea Level Rise) percentile scenarios, for 2060-2080 and 2080-2100 respectively. The blue regions represent the areas with water height larger than $15cm$. d: Original network without sea level rise, in an abstract network space representation. Notice that facilities do not link directly to each other, but connect through transportation nodes (road and pipelines). e and f: Network including nodes unaffected by sea level rise, at RCP 8.5 and 99.9 SLR percentile scenario, for the period 2060-2080 and 2080-2100, respectively.

Parameter	Values
N_1	5
N_2	29
N_3	3422
C^1	$[38.2, 57.3]$ Mgal
C^2	$[31, 62]$ Mgal
C^3	0.035 Mgal
W^{12}	$[70, 140]$ Mgal week^{-1}
W^{23}	$[105, 245]$ Mgal week^{-1}
W^{13}	$[21, 81]$ Mgal week^{-1}
P	18.9 Mgal week^{-1}
D	0.028 Mgal week^{-1}

Table 1. Parameters representing the aggregated characteristics of the SFFTN. $W^{qr} = \sum_{i=1}^{N_q} \sum_{j=1}^{N_r} W_{ij}^{qr}$ represents the aggregated flow capacity between layers q and r. By considering ranges for some of the parameters we are able to capture a reasonable range of scenarios for the network description. See Methods section for more details.

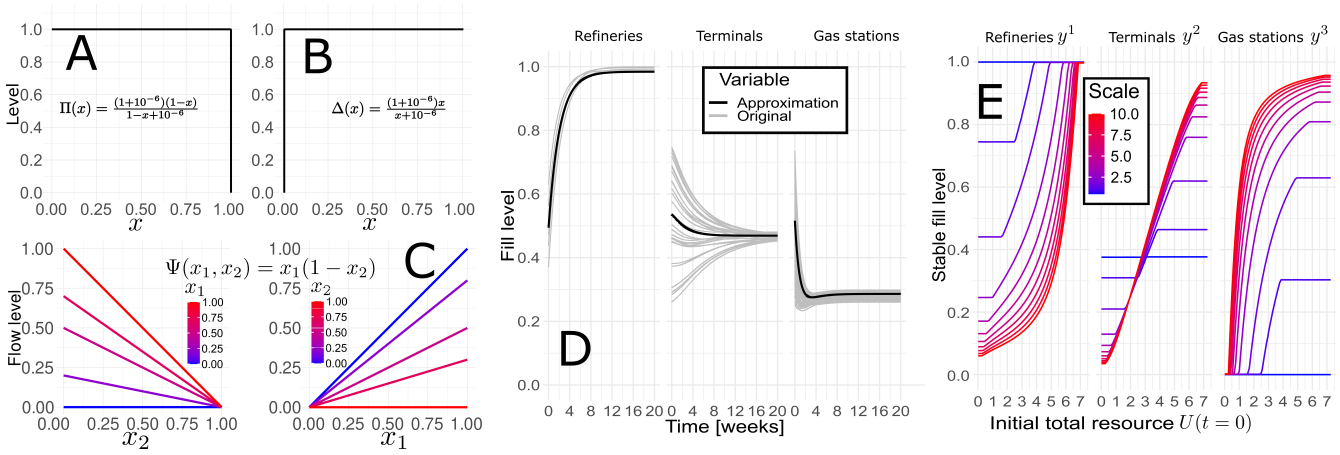

Figure 2. Dynamical representation considered. a: Production level Π as function of stock level x. The function captures maximal production except when stock level $x \approx 1$. b: Demand level Δ as a function of stock level x. The function captures constant demand except for $x \approx 0$. c: Flow level, as a function of sender and receiver stock levels, x_1 and x_2. The flow is greater for high stock levels of the sender or low stock levels of the receiver. d: Dynamical evolution for a system with 5 refineries, 29 terminals, and a random sample of 100 gas stations. All layers are considered fully connected, and flow capacities are constant and equal to $W^{qr}/N_q N_r$ between nodes in layers q and r. Black solid lines represent the stock level estimated by the approximation. e: The stable values of stock levels y^q for each layer calculated using the approximation, as a function of the initial total resource $U(t=0) = y^1(t=0) + \alpha_{12} y^2(t=0) + \alpha_{12}\alpha_{23} y^3(t=0)$ and the flow capacities of the network. Scale (in legend) represents the transformation of flow capacities respect to their average values. At a given scale S, the flow capacities are $S \times s_{qr}$. Notice how the stable stock levels increase for higher values of $U(t=0)$. The maximum and minimum possible stock levels are limited by the flow capacities in the network, exemplified the change in scale. For low values of $U(t=0)$ and scale S, the third layer may get empty, producing a demand failure.

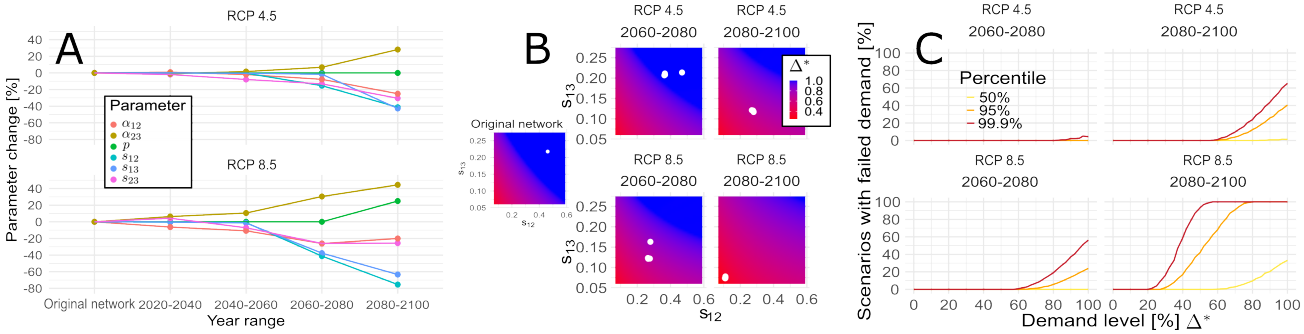

Figure 3. Demand stability under different sea level rise scenarios. a: Parameter as percent of their original values, for the different time horizons and for the two Representative Concentration Pathways (RCPs) considered. As the Sea Level Rise (SLR increases, changes are more evident. Note that a_{23} increases because coastal flooding affects terminals more than gas stations. Also, p increases due to the flooding at one refinery, under the assumption of equal total production at every scenario. b: Demand diagrams in terms of s_{12} and s_{13} for the original network and the last two time horizons, where demand failure occurs. Each white dot corresponds to the average values of the flow capacities s_{12} and s_{13} under the prediction of each Global Climate Model (GCM), for the corresponding time horizon and RCP value. Notice how the values of s_{12} and s_{13} move toward the region of demand failure, but also the region of demand failure increases. To construct the diagrams, the average value of s_{23}, α_{12}, α_{23}, p and d for each scenario are used. Panels a and b correspond to the 99.9 SLR percentile. c: Percentage of network scenarios (considering the range of possible values for each parameter) with failed demand, as a function of the desired demand level Δ^*.

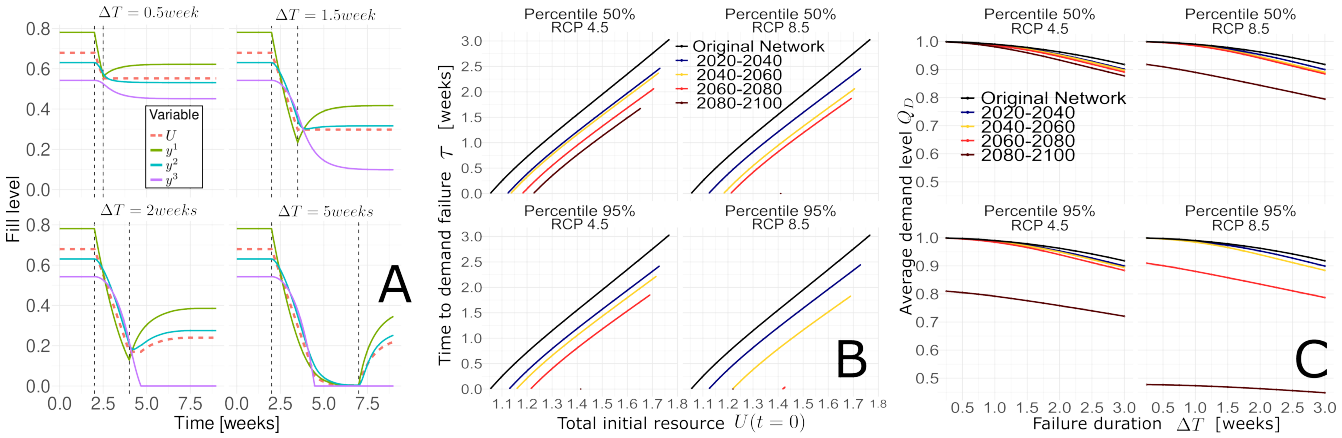

Figure 4. Dynamics of production failure under Sea Level Rise scenarios. a: To simulate a full production failure, we initialize the system at a stable state, and set $p = 0$ during a time ΔT. The stock levels decrease and demand failure may be reached if $y^3 \approx 0$. Notice that y^3 may still reach 0 even after the failure ended. The plot shows stock level of layer 1 (green), layer 2 (cyan) and layer 3 (magenta), and total stock level (dashed pink line). b: For the Sea Level Rise (SLR) at 50 and 95 percentiles, we calculate the time τ it takes the system to reach demand failure as a function of the resource stored on it. The change in the parameters reduce the values of τ for a given amount of resource. Even more, the range of total resource that the system can store also reduces. The color scale indicates the time horizons: original (black), 2020-2040 (red), 2040-2060 (orange), 2060-2080 (light green) and 2080-2100 (blue). c: Average demand level Q_D as a function of the failure duration. For low failure duration times, the system is able to resist failure and sustain maximum demand. For long failure duration times demand failure occurs, reducing the average demand. While for short failure duration the SLR affects similarly the average demand, the effect increases for the last time horizons (green and blue lines). For RCP 8.5 and high percentiles, the effect is so drastic that the average demand decreases for any failure duration in the last horizon (RCP 4.5) and the two last horizons (RCP 8.5). The same color scale applies for panels b and c.

Parameter	Values
α_{12}	$[3.14, 9.41]$
α_{23}	$[0.07, 0.13]$
s_{12}	$[0.25, 0.79]$ week^{-1}
s_{23}	$[0.05, 0.27]$ week^{-1}
s_{13}	$[0.17, 0.43]$ week^{-1}
p	$[0.33, 0.49]$ week^{-1}
d	0.79 week^{-1}

Table 2. Normalized parameters capturing realistic values for the SFFTN The ranges of values are obtained from the ranges in the natural parameters in Table 1

	N_1	N_2	N_3	Min-Cut	$f_{13}[\%]$	$f_{23}[\%]$
Original	5	29	3422	5	1	1
Representative Concentration Pathway (RCP) 4.5						
2020-2040	5	[26,28]	[3369,3388]	5	[98.1,98.7]	[80.6,88.2]
2040-2060	5	[25,26]	[3359,3377]	5	[97.7,98.3]	[73.3,87.8]
2060-2080	5	[23,26]	[3315,3368]	[4,5]	[96.4,98.1]	[65.4,80.6]
2080-2100	5	[19,25]	[3225,3346]	[3,5]	[55.8,97.6]	[43.2,76.7]
Representative Concentration Pathway (RCP) 8.5						
2020-2040	5	[26,27]	[3371,3382]	5	[98.2,98.4]	[80.7,87.9]
2040-2060	5	[24,26]	[3324,3379]	5	[96.8,98.3]	[72.6,87.8]
2060-2080	5	[20,25]	[3248,3356]	[3,5]	[56.4,97.9]	[47,76.9]
2080-2100	[4,5]	[17,22]	[3117,3292]	[1,3]	[36,95.6]	[41.7,51.2]

Table 3. Change of the network structure through the different time horizons, for the two Representative Concentration Pathways considered. The ranges of values correspond to the predictions of the four Global Climate Models and the three Sea Level Rise percentiles. N_1, N_2 and N_3 correspond to the number of refineries, terminals and gas stations. Min-cut corresponds to the minimum cut to separate all refineries from all terminals. f_{13} is the average fraction of gas stations that are accessible from a refinery through the road network. f_{23} is the average fraction of gas stations that are accessible from a terminal through the road network.